Kinetic parameters of the dissociation of $Nd_2Fe_{14}B$ during oxidation determined by Mössbauer spectrometry

1996 J. Phys.: Condens. Matter 8 10721

(http://iopscience.iop.org/0953-8984/8/49/056)

J. Phys.: Condens. Matter **8** (1996) 10721–10736. Printed in the UK

Kinetic parameters of the dissociation of $Nd_2Fe_{14}B$ during oxidation determined by Mössbauer spectrometry

S Steyaert, J M Le Breton and J Teillet

Laboratoire de Magnétisme et Applications, URA CNRS 808, Faculté des Sciences de l'Université de Rouen, 76821 Mont-Saint-Aignan Cedex, France

Received 9 July 1996, in final form 5 September 1996

Abstract. Powdered Nd–Fe–B permanent magnets were sieved to different particle sizes and oxidized in an ambient air furnace in the 150–300 °C temperature range for different times. Transmission Mössbauer spectrometry was used to determine the dissociation kinetics of the $Nd_2Fe_{14}B$ phase. The experimental curves were fitted according to the Ginstling–Brounshtein model, taking into account the real distribution of particle size. The kinetic parameters, namely the activation energy E_a and the diffusivity pre-exponential factor D_0 were determined to be 110 kJ mol^{-1} and 2.4 mm^2 s^{-1} respectively, It appeared that the kinetics parameters could be determined as well by considering a simple theoretical single-particle analysis model. The influence of the particle size was studied in the case of this simple model.

1. Introduction

In spite of their good magnetic properties, the use of Nd–Fe–B permanent magnets is still restricted by their poor corrosion resistance. Sintered Nd–Fe–B magnets are constituted of three phases: the $Nd_2Fe_{14}B$ major phase, the non-magnetic $Nd_{1.1}Fe_4B_4$ phase and a Nd-rich intergranular phase. According to published results, the corrosion behaviour of these phases is the following. The Nd-rich phase (responsible for the good coercivity of the magnet) is very sensitive to corrosion, being rapidly affected by humidity [1]. The nature of the corrosion products (Nd_2O_3 or $Nd(OH)_3$) depends both on temperature and on humidity [2]. The $Nd_2Fe_{14}B$ phase oxidizes slowly at around 100 °C and its oxidation rate increases with temperature [2, 3]. The oxidation mechanism of the $Nd_2Fe_{14}B$ phase has recently been characterized by transmission electron microscopy: the Nd is oxidized and the phase dissociates into nanoparticles of iron, which grow epitaxially from $Nd_2Fe_{14}B$ substrate [4]. On the other hand, the $Nd_{1.1}Fe_4B_4$ phase is not oxidized, even at 400 °C [5].

To increase the intrinsic corrosion resistance, it is possible to use additives which form corrosion resistant intergranular or intragranular precipitates (Co, Zr, V...) [6]. The use of coatings increases the lifetime of the magnet, but, when the corrosion starts, it occurs below the coating/magnet interface, so that the corrosion mechanism of the coated magnet is related to the corrosion mechanism of the uncoated magnet [7]. In order to estimate the lifetime of a Nd–Fe–B magnet at high temperature, it appears to be necessary to determine the oxidation kinetic parameters of the $Nd_2Fe_{14}B$ phase, because the degradation of the magnetic properties at high temperature is related to the dissociation of this phase [8].

With the aim of determining the activation energy and the diffusivity pre-exponential factor of the dissociation process of the $Nd_2Fe_{14}B$ phase in the 150–300 °C temperature range, we followed the evolution of the $Nd_2Fe_{14}B$ phase by ^{57}Fe Mössbauer spectrometry.

0953-8984/96/4910721+16$19.50

This technique was shown to be a very useful tool for such a study, because the $Nd_2Fe_{14}B$ contribution to the Mössbauer spectrum is about 95% for an untreated magnet [6].

2. The experimental procedure

$Nd_{16}Fe_{76}B_8$ sintered magnets were supplied by the University of Birmingham (UK). They were powdered and sieved to the following particle sizes: less than 20, 20–40, 40–63 and 63–100 μm. The particle size distribution was measured by scanning electron microscopy (SEM). The powders were oxidized in an ambient air furnace at temperatures in the range 150–300 °C for different times. Heat-treated samples were then analysed by transmission Mössbauer spectrometry (TMS) at room temperature. This technique allows the volume of the particle to be analysed. Transmission Mössbauer analysis was performed using a conventional ^{57}Co source in a rhodium matrix. The isomer shift (relative to metallic α-Fe at room temperature), quadrupolar splitting, quadrupolar shift and hyperfine field are denoted IS, QS, 2ϵ and H_{hf} respectively. Estimated errors Δ for hyperfine parameters originate from the statistical errors σ given by the fitting program [9], taking $\Delta = 3\sigma$.

3. Fitting of the Mössbauer spectra

All the Mössbauer spectra were fitted with a procedure which was described previously [6]. This procedure can be summarized as follows. First, the hyperfine parameters both of the $Nd_2Fe_{14}B$ and of the $Nd_{1.1}Fe_4B_4$ phase were fixed to the values obtained from the Mössbauer spectrum of the untreated sample. Next, the hyperfine parameters of the corrosion products were fixed to the values obtained from the Mössbauer spectrum of a completely corroded sample (the values obtained for the hyperfine parameters are reported in table 1). Then, throughout the spectra, the relative intensities of the contributions to the Mössbauer spectra of the corroded samples (from $Nd_2Fe_{14}B$, $Nd_{1.1}Fe_4B_4$ and corrosion products) were fitted, keeping their hyperfine parameters constant to the values obtained before. The Mössbauer spectra at 300 °C are displayed in figure 1.

Table 1. Room temperature hyperfine parameters.

Sub-spectrum	H_f (T)	IS (mm s^{-1})	2ϵ, QS (mm s^{-1})
$Nd_2Fe_{14}B$			
$16k_1$	28.0 ± 0.2	-0.06 ± 0.01	0.27 ± 0.01
$16k_2$	30.2 ± 0.2	-0.11 ± 0.01	0.13 ± 0.01
$8j_1$	26.0 ± 0.2	-0.08 ± 0.01	0.23 ± 0.01
$8j_2$	33.9 ± 0.2	0.07 ± 0.01	0.61 ± 0.01
$4e$	26.6 ± 0.2	-0.12 ± 0.01	-0.32 ± 0.02
$4c$	23.6 ± 0.2	-0.05 ± 0.01	0.09 ± 0.02
$Nd_{1.1}Fe_4B_4$		0.02 ± 0.01	0.52 ± 0.02
Corrosion products			
α-Fe (distribution)	33.3 ± 0.2	0.00 ± 0.02	0.00 ± 0.02
Magnetic distribution	36.8 ± 0.4	0.34 ± 0.02	-0.10 ± 0.02
α-Fe_2O_3	51.2 ± 0.2	0.32 ± 0.01	-0.23 ± 0.01
Paramagnetic doublet		0.40 ± 0.02	0.85 ± 0.05

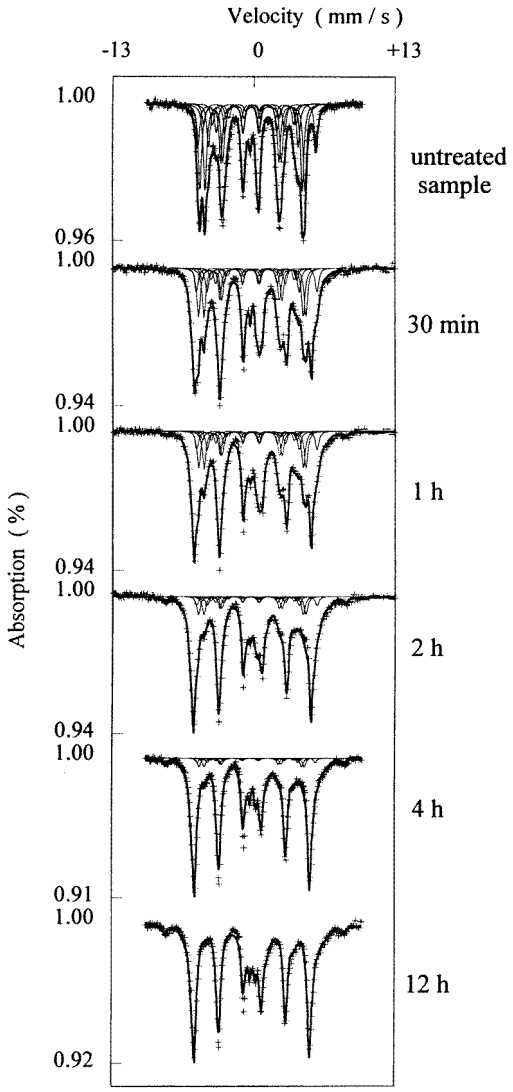

Figure 1. Room temperature Mössbauer spectra of samples heated at 300 °C. The contribution (six sextets) of the $Nd_2Fe_{14}B$ phase is displayed.

The contributions of the corrosion products were analysed in relation to the dissociation process of the $Nd_2Fe_{14}B$ phase. The details of this interpretation will be described elsewhere [10].

The Mössbauer relative intensity of the $Nd_2Fe_{14}B$ phase (related to the number of iron atoms in the phase) was determined for different treatment times. For each temperature, the experimental $R_\phi = f(t)$ curve was plotted, t being the treatment time and R_ϕ being defined by

$$R_\phi(t) = \frac{\phi(t)}{\phi(t=0)} \times 100 \tag{1}$$

where $\phi(t)$ is the relative intensity of the $Nd_2Fe_{14}B$ phase contribution to the Mössbauer spectrum after t days at a given temperature.

By assuming that the Lamb–Mössbauer factors of the different phases are equal, the ratio $\phi(t)/\phi(t=0)$ is equal to the volume of the $Nd_2Fe_{14}B$ phase (ϕ phase) after t days of treatment time $V_\phi(t)$ compared to the initial volume $V_\phi(t=0)$. Thus, at each time t, $R_\phi(t)$ represents the unreacted fraction of the material and the $R_\phi = f(t)$ curves show the disappearance in volume of the $Nd_2Fe_{14}B$ phase:

$$R_\phi(t) = \frac{V_\phi(t)}{V_\phi(t=0)} \times 100. \tag{2}$$

4. Fitting of the experimental $R_\phi = f(t)$ curves

4.1. The theoretical model

Because microstructural observations revealed that the particles sieved are roughly spherical (figure 2), we applied a model that considers the uni-directional diffusion through a sphere (the so-called 'contracting envelope' or 'shrinking core' [11]). This model assumes that the oxidation process is governed by oxygen diffusion through the corrosion product layer which continues to adhere to the unoxidized part of the particle. These assumptions are valid in the case of Nd–Fe–B magnets, as was shown by microstructural observations of bulk magnets oxidized in air at 400 °C [5].

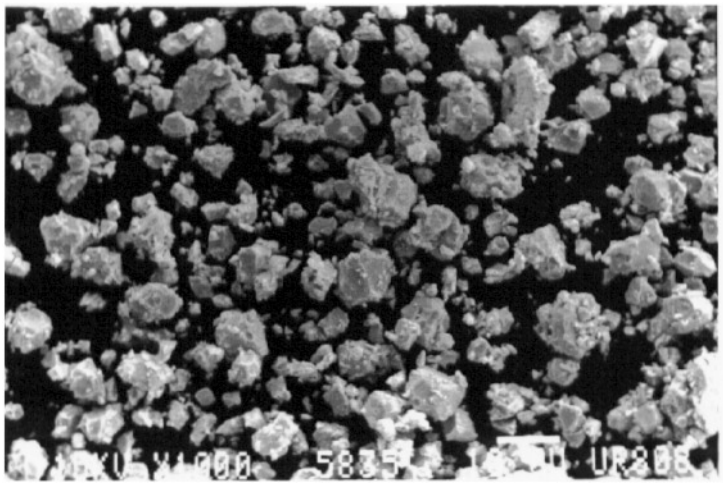

Figure 2. A SEM image of particles for a powder sieved to less than 20 μm.

In order to fit the experimental $R_\phi = f(t)$ curves with the best possible accuracy, we used the Ginstling–Brounshtein model in which we introduced the real particle size distribution of powders, measured by SEM. The Ginstling–Brounshtein model, which is a single-particle analysis model, considers the growth of the product layer for steady-state distribution of concentration through a spherical shell, the volume of the product layer being equal to the volume of reactant consumed [11].

The oxygen concentration at the surface of the particles can reasonably be assumed constant. On the other hand, micro-analysis measurements performed on oxidized magnets

showed that the oxygen concentration remains constant at the interface between the oxidized area and the non-oxidized area [4, 5, 12].

Concerning the possible volume change occurring during the reaction process, Geiss showed that the Ginstling–Brounshtein equation is significant when the ratio of the volume of product formed to the volume of reactant consumed is lower than two [13]. According to previous results [12], no significant volume change occurs during the oxidation process of the $Nd_2Fe_{14}B$ phase and thus this model is applicable.

For a sphere of radius r, the reaction kinetics is characterized by the following equation [11]:

$$\frac{2D(T)}{r^2}t = 1 - \frac{2}{3}\alpha(t) - (1-\alpha(t))^{2/3} \tag{3}$$

where $\alpha(t)$ is the reacted fraction at time t and $D(T)$ is the diffusivity at temperature T. The oxidation process being thermally activated, $D(T)$ can be written according to Arrhénius law:

$$D(T) = D_0 \exp\left(\frac{-E_a}{RT}\right) \tag{4}$$

where E_a is the activation energy, R the rare gas constant, T the absolute temperature and D_0 the diffusivity pre-exponential factor.

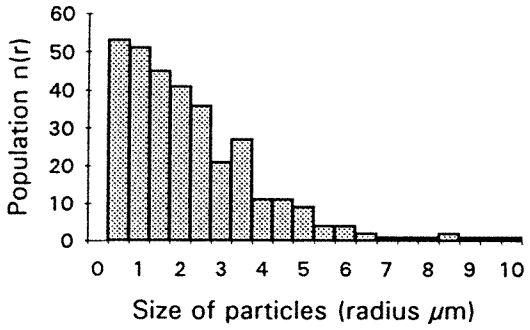

Figure 3. The particle size distribution for powders sieved to less than 20 μm measured by SEM.

In figure 3 is shown the distribution of particle size: there are 20 classes of particles of radius r_i ($0.5\ \mu\text{m} \leqslant r_i \leqslant 10\ \mu\text{m}$) and $n(r_i)$ is the number of particles for the class i. Therefore, from the choice of a couple of values (E_a, D_0), the equation (3) is solved for each class of particles. For the class i, the equation (3) is

$$\frac{2D(T)}{r_i^2}t = 1 - \frac{2}{3}\alpha_i(t) - (1-\alpha_i(t))^{2/3}. \tag{3'}$$

If we consider $R_{\phi_i}(t)$ the unreacted fraction at time t of a particle of the class i, $R_{\phi_i}(t)$ is equal to $1-\alpha_i(t)$ and, by writing $\xi_i(t) = R_{\phi_i}(t)^{1/3}$ and substituting it into equation (3′), the following equation is obtained:

$$\xi_i^3 - 1.5\xi_i^2 + \left(0.5 - \frac{3D(T)}{r_i^2}t\right) = 0 \tag{5}$$

whose physically meaningful root is [14]

$$\xi_{i_0} = 0.5 + \cos\left[\tfrac{1}{3}\cos^{-1}\left(\frac{12D(T)}{r_i^2}t - 1\right) + \tfrac{4}{3}\pi\right] \qquad \text{for } 0 \leqslant t \leqslant t_i \tag{5'}$$

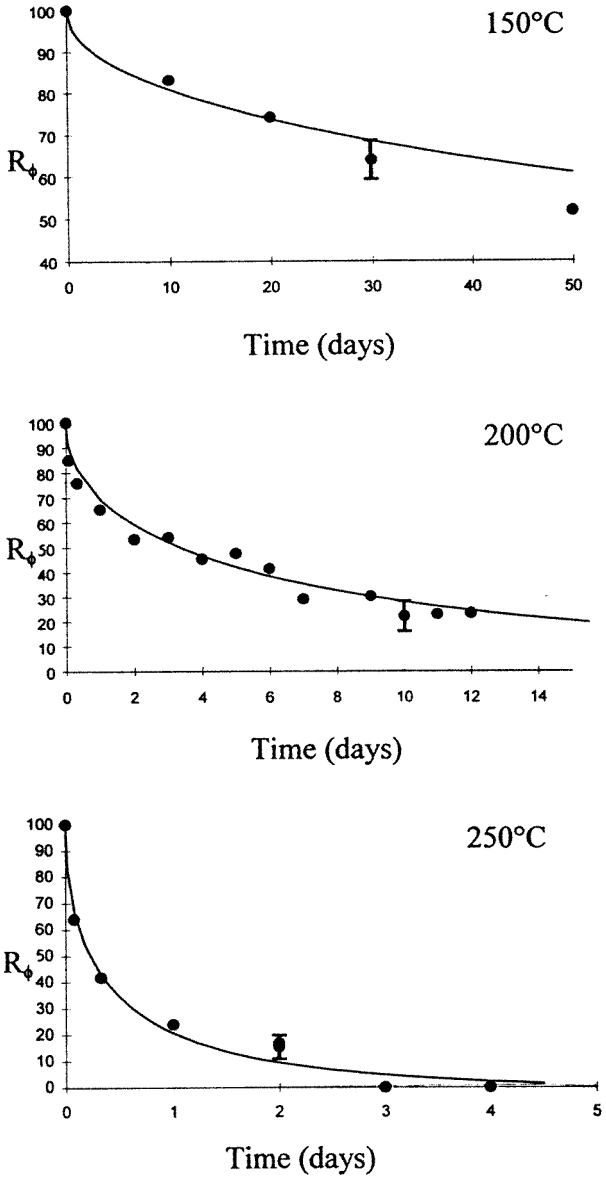

Figure 4. Experimental points and fitted curves obtained from the Ginstling–Brounshtein model extended to a particle size distribution for powders sieved to less than 20 μm.

$t_i = r_i^2/(6D(T))$ being the time corresponding to the complete oxidation of a particle of class i.

Then, for each class i, the value $R_{\phi_i}(t)$ is equal to $\xi_{i_0}^2(t)$. Next, R_ϕ defined by equation (2) is obtained from the following equation:

$$R_\phi(t) = \frac{\sum_j R_{\phi_j}(t) \times V_j(t=0) \times n(r_j)}{\sum_{i=1}^{i=20} V_i(t=0) \times n(r_i)} \times 100 \tag{6}$$

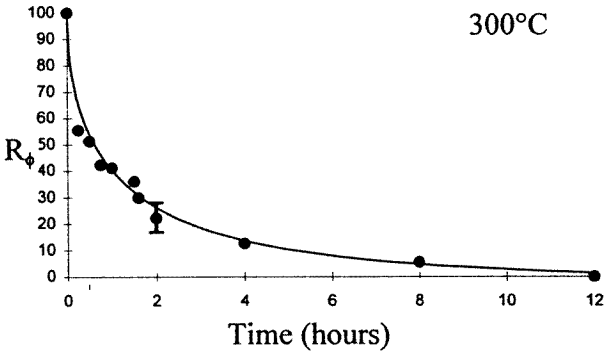

Figure 4. (Continued)

where the index j concerns only the classes of particles which had not totally oxidized at time t, $V_j(t = 0)$ being the volume of the unoxidized particle j.

The experimental $R_\phi = f(t)$ data were thus fitted according to equation (6). Different couples (E_a, D_0) were tested in order to find the best fit to the experimental points.

Finally, it must be noted that, when the particles are not perfectly spherical, this kind of model is applicable and the experimental results are consistent with the model, as indicated by Valensi [15]. Moreover, Mintz and Zeiri studied with high accuracy the effect of particle shape and concluded that little variations in the particle shape do not alter this type of analysis much [14].

4.2. Determination of the kinetic parameters: results and discussion

4.2.1. Results obtained for powders sieved to less than 20 μm. From the distribution of particle size measured by SEM, shown in figure 3, only a few particles have a diameter greater than 10 μm. In bulk magnets, the size of the $Nd_2Fe_{14}B$ grains is about 10–15 μm, so most of the particles are composed of a fraction of a grain. Therefore, what is observed in the $R_\phi = f(t)$ curves is the oxidation of particles containing pure $Nd_2Fe_{14}B$ phase with no grain boundary inside. Consequently, the kinetic parameters E_a and D_0 are those of the pure dissociation of the $Nd_2Fe_{14}B$ phase, namely the purely intragranular diffusion process.

The couple of values (E_a, D_0) which fits the experimental $R_\phi = f(t)$ curves best was determined to be $E_a = 110$ kJ mol^{-1}, $D_0 = 2.4$ mm^2 s^{-1} and the related curves are shown in figure 4. From the different fittings achieved by varying the values of E_a and D_0, the accuracies were estimated to be 10 kJ mol^{-1} and 1.8 mm^2 s^{-1} respectively.

With the aim of using a simpler model considering a distribution of identical spherical particles, we applied Jander's model [16]. In this model, the thickness of the oxidized shell is assumed to follow a time-parabolic law, similar to the diffusion-controlled planar case. Many authors [14, 17] discarded this model (when applied to the case of spherical particles), arguing that the assumption of the parabolic time-dependence of the oxidized layer thickness is incorrect since the surface area is not constant, or indicated that Jander's model is only applicable during the first stages of the reaction process, when the thickness of the oxidized layer is far lower than the radius of the particle. Here we investigated the validity range of Jander's model.

By introducing directly the thickness x of the spherical oxidized layer in the expression

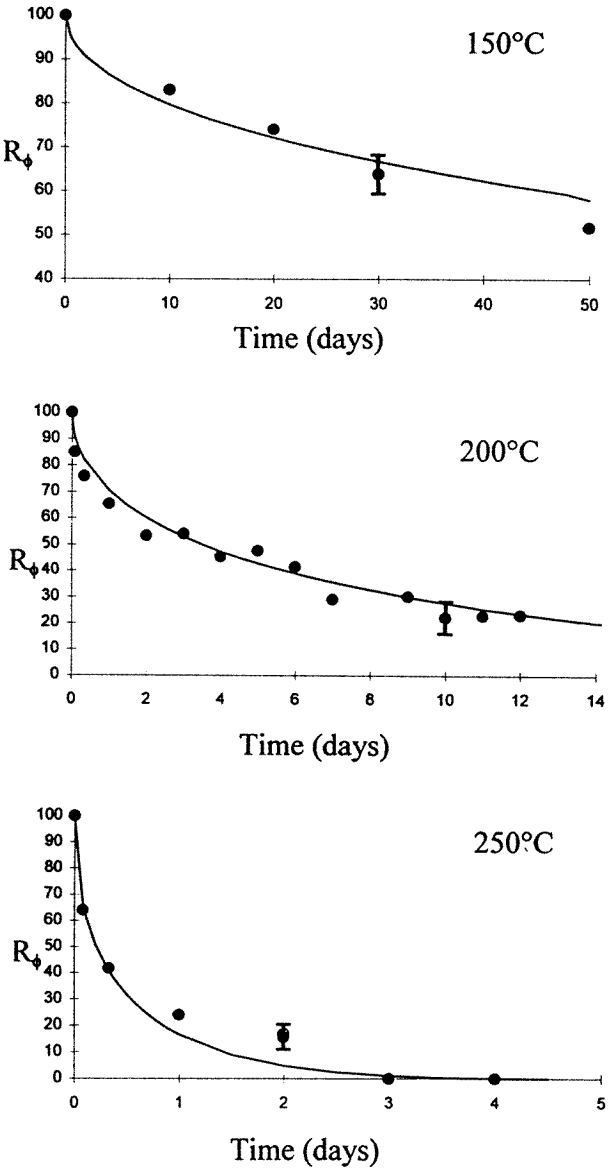

Figure 5. Experimental points and fitted curves obtained from Jander's model for powders sieved to less than 20 μm.

for $R_\phi(t)$ given in equation (2), R_ϕ is simply written

$$R_\phi(t) = \left(1 - \frac{x(t)}{r}\right)^3 \times 100 \tag{7}$$

where r is the radius of the spherical particle. Then, writing that

$$x^2(t) = 2D(T) \times t \tag{8}$$

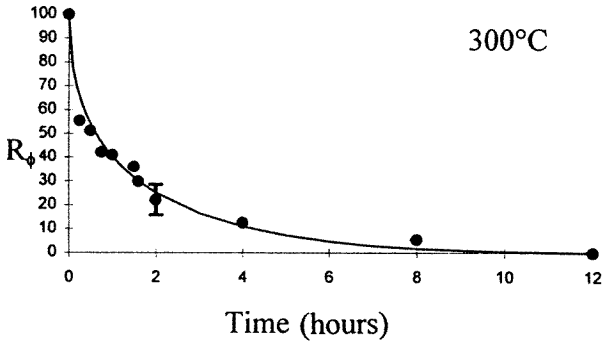

Figure 5. (Continued)

$D(T)$ being the diffusivity, the expression for R_ϕ becomes

$$\left(\frac{R_\phi}{100}\right)^{1/3} = 1 - \left(\frac{(2D(T))^{1/2}}{r}\right)\sqrt{t}. \tag{9}$$

Consequently, the experimental points were fitted with equation (9) and we obtained satisfactory fittings (figure 5). The value of the activation energy E_a (which requires no assumption concerning the size of the single particle of Jander's model) can be deduced from the slope of the $\ln(2D(T)/r^2) = f(1/T)$ curve (figure 6). A value of 109 kJ mol^{-1} was obtained which is very consistent with the value obtained from the Ginstling–Brounshtein model extended to a particle size distribution.

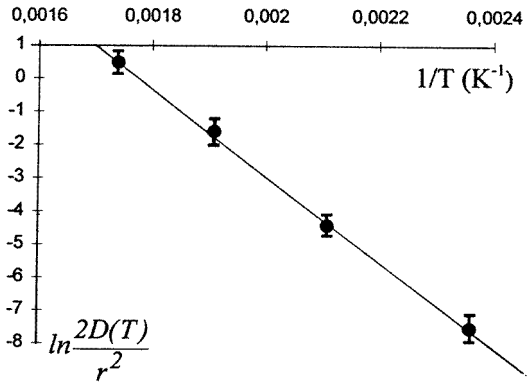

Figure 6. The Arrhénius plot obtained from Jander's model for powders sieved to less than 20 μm ($E_a = 109$ kJ mol^{-1}).

Then, the values of $R_\phi^{1/3}$ were plotted versus $\sqrt{t}$ (figure 7), R_ϕ being calculated from the extended Ginstling–Brounshtein model. From these curves, it appears that $R_\phi^{1/3} = f(\sqrt{t})$ is a linear function as long as R_ϕ is greater than 30%. Then, Jander's model is equivalent to the Ginstling–Brounshtein model for a large R_ϕ range (30–100%). Moreover, within the experimental errors, the two models give comparable results (error bars in figure 7). It is possible to estimate the size of the single spherical particle of Jander's model from the zero ordinate of the $\ln(2D(T)/r^2) = f(1/T)$ curve by assuming that D_0 is equal to the value

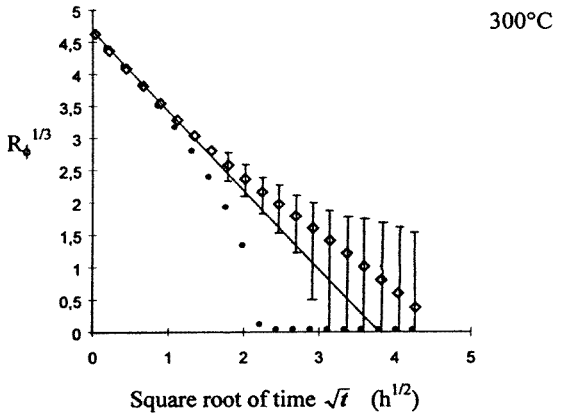

Figure 7. $R_\phi^{1/3}$ versus $\sqrt{t}$ points for powders sieved to less than 20 μm: the Ginstling–Brounshtein model (◊) extended to a distribution of particle size and (●) applied to a single spherical particle. The full line represents the simple version of Jander's model.

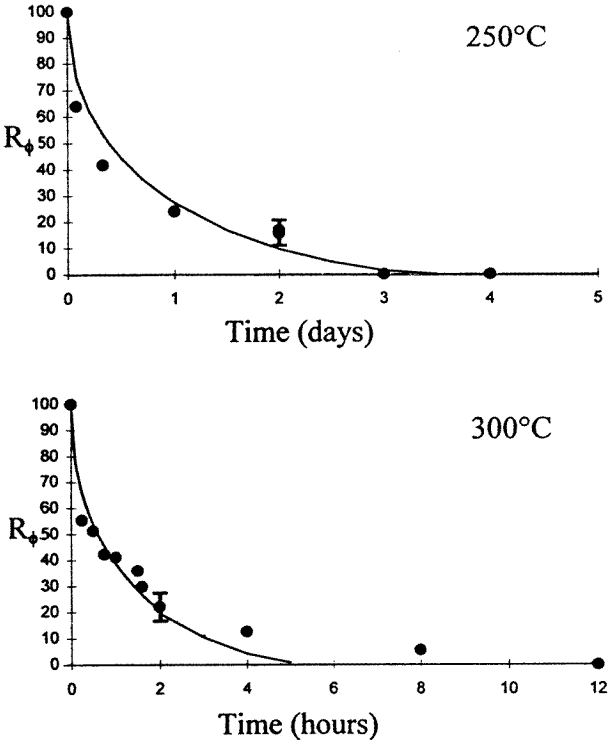

Figure 8. Experimental points and fitted curves obtained from the Ginstling–Brounshtein single-particle analysis model for powders sieved to less than 20 μm at 250 and 300 °C.

obtained with the extended Ginstling–Brounshtein model. The value of r was determined to be about 5 μm.

It must be noted that the use of the Ginstling–Brounshtein single-particle analysis model

(without considering the real particle size distribution) gives fittings of the experimental $R_\phi = f(t)$ curves which are not so satisfactory as those obtained with both the two previous models (figure 8). From the comparison of these models, it appears that Jander's model can be applied for a large R_ϕ range (30–100%), the corresponding radius of the single spherical particle being 5 μm. The fact that the validity range of Jander's model is large may be due to the effect of the particle size distribution. The fitting of the experimental points according to Jander's model seems to compensate for the effect of the real particle size distribution, which is not taken into account (and does not need to be measured) in Jander's single-particle analysis model. From the $R_\phi^{1/3}$ versus $\sqrt{t}$ points calculated from this model, it is clear that the Ginstling–Brounshtein single-particle analysis model is farther from the Ginstling–Brounshtein model extended to a distribution of particle size than is Jander's model. Consequently, Jander's model, which accounts well for the intragranular diffusion in Nd–Fe–B magnets (provided that the R_ϕ range remains between 100% and about 30%), was retained and used in order to follow the oxidation behaviour of particles sieved to larger than 20 μm.

4.2.2. Results obtained for powders sieved to 20–40, 40–63 and 63–100 μm. In order to characterize the influence of particle size on the determination of the kinetic parameters, powders sieved to a size larger than 20 μm were oxidized at 300 °C. According to the conclusions of section 4.2.1, the experimental points were fitted (for the values of R_ϕ higher than 30) by considering a distribution of identical spherical particles of radius r and the fitted $R_\phi = f(t)$ curves obtained from Jander's model are reported in figure 9. This model allows the experimental data to be fitted correctly.

Since the mean $Nd_2Fe_{14}B$ grain size in the bulk magnet is about 10–15 μm, the particles of each type of powder are composed of several $Nd_2Fe_{14}B$ grains. These particles have the same composition as that of the particles of size less than 20 μm and we can assume that both the activation energy and the diffusivity of the intragranular diffusion process are equal to the values obtained before.

Then, from the slope of the experimental $R_\phi^{1/3} = f(\sqrt{t})$ curves at 300 °C, it is possible to estimate the diameter of the spherical particle of the theoretical model (namely the diameter of the spherical particle which oxidizes). The results are 16 μm for the 20–40 μm powders, 20 μm for the 40–63 μm powders and 45 μm for the 63–100 μm powders. In each case, the diameter of the spherical particle of the theoretical model is far lower than the size of the particles in the powders.

The first value (16 μm) is similar to the $Nd_2Fe_{14}B$ grain size. Consequently, Jander's model applies if the spherical particle is a $Nd_2Fe_{14}B$ grain. These results are consistent with the results obtained for powders sieved to less than 20 μm, if we consider that the Nd-rich intergranular phase and the grain boundaries are preferential paths of diffusion for oxygen. Thus, from the first stage of oxidation, the edge of the $Nd_2Fe_{14}B$ grains is rapidly affected by oxygen (this is indicated in figure 10), indicating that the intergranular diffusion process is the dominant process. The following stages of the oxidation process are governed by the intragranular diffusion of oxygen and the kinetic parameters that it is possible to measure are those of the dissociation of the $Nd_2Fe_{14}B$ phase.

For the 40–63 and 63–100 μm powders, the diameters of the theoretical spherical particles (20 and 45 μm respectively) are found to be greater than the grain size. This result is attributed to the fact that the diffusion of oxygen through the Nd-rich phase is not fast enough to allow the $Nd_2Fe_{14}B$ grains in the centre of the particle to be affected from the beginning of the treatment. This is illustrated in figure 11. Thus, for such big particles,

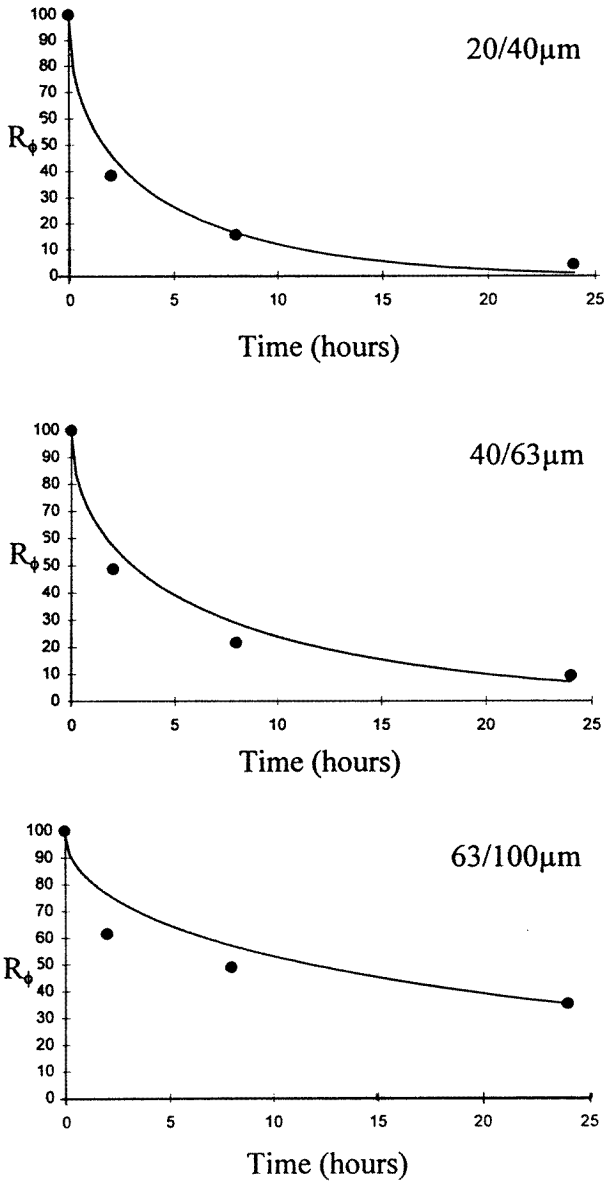

Figure 9. Experimental points and fitted curves obtained from Jander's model for powders sieved to more than 20 μm at 300 °C.

what is observed is the effect both of intergranular and of intragranular diffusion processes so that the value obtained for the diameter of the spherical particle is not representative and thus the simple theoretical model does not apply.

In figure 12 is shown the well-known schematic temperature variation of the diffusivity in bulk Nd–Fe–B sintered magnets with both intragranular and intergranular diffusion contributions (the intragranular contribution corresponding to the dissociation of the $Nd_2Fe_{14}B$ phase). In a bulk magnet, for temperatures less than the cross over temperature T_i,

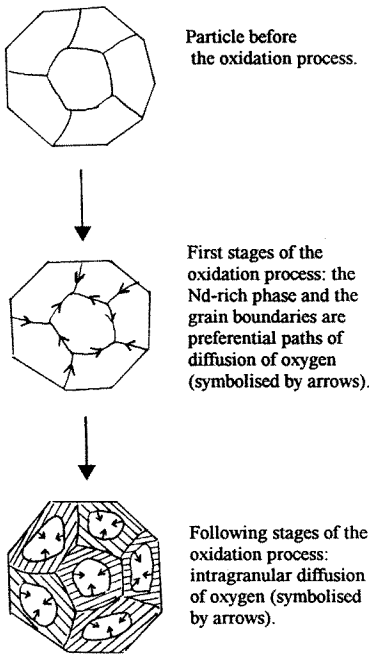

Figure 10. The oxidation process at 300 °C for the 20–40 μm powders.

the intergranular diffusion contribution dominates whereas, for temperatures greater than the cross over temperature, the intragranular diffusion dominates. From considering the results of different studies [3], the cross over temperature should be located in the range 280–360 °C. Our results indicate that the intergranular diffusion process still dominates at 300 °C indicating that the cross over temperature in bulk sintered magnets should be greater than 300 °C. These results show that the kinetic parameters of the dissociation of $Nd_2Fe_{14}B$ can be determined unambiguously for powders with particle size less than the grain size.

5. Discussion

The kinetic parameters E_a and D_0 of the dissociation process of the $Nd_2Fe_{14}B$ phase ($E_a = 110$ kJ mol^{-1} and $D_0 = 2.4$ mm^2 s^{-1}) determined by transmission Mössbauer spectrometry are in good agreement with SEM measurements of the thickness of the oxidized layer performed on bulk magnets in the 360–600 °C temperature range [8, 12]. Edgley *et al* [12] reported an activation energy of 114 ± 11 kJ mol^{-1} and a diffusivity pre-exponential factor of 0.7 mm^2 s^{-1}. The value of the activation energy is consistent too with the value of 118 kJ mol^{-1} measured by Blank and Adler [8]. In fact, they found 59 kJ mol^{-1}, but defined the activation energy E'_a with the following equation:

$$k(T) = k_0 \exp\left(\frac{-E'_a}{RT}\right)$$

the thickness of the oxidized layer $x(t)$ being

$$x(t) = k(T) \times \sqrt{t}.$$

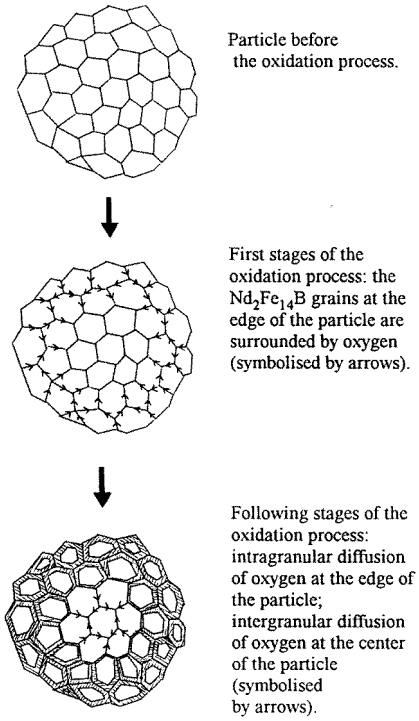

Figure 11. The oxidation process at 300 °C for the 40–63 and 63–100 μm powders.

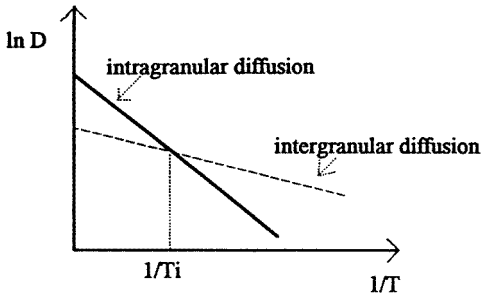

Figure 12. The schematic temperature variation of the diffusivity in bulk sintered Nd–Fe–B magnets.

Thus, $D(T)$ is proportional to $k^2(T)$ and the value of the activation energy that must be considered has to be multiplied by two. In each case, it was found that the measured thickness of the dissociated layer depends on the square root of time, which is consistent with an oxygen diffusion process throughout the corrosion product layer. The results obtained here show that the phenomenon followed by Mössbauer spectrometry and SEM is the same. This is illustrated in figure 11. At high temperature, for which the intragranular diffusion is the dominant process, the advance of the oxidation front is significant and can be measured by SEM or optical microscopy. At low temperature, the thickness of the oxidized layer

is no longer significant and cannot be measured by SEM. Furthermore, the intergranular diffusion becomes the dominant process. Consequently, a Mössbauer study on powders sieved to less than 20 μm which are free from the intergranular phases allows the kinetics of the pure intergranular diffusion to be determined.

Stewart *et al* [18] determined the oxidation kinetic parameters of Nd–Fe–B powders by thermogravimetric measurements in the 20–1100 °C temperature range. They fitted the experimental curves by taking into account the distribution of particle size with the assumption of a parabolic time-dependence of the thickness of the oxidized layer and reported an activation energy of 100 kJ mol^{-1}. Because measurements in the 20–1100 °C range include the oxidation of iron (above 400 °C), this value does not correspond to the pure dissociation of the $Nd_2Fe_{14}B$ phase. However, this value is close to the value obtained in our study because it appears that the activation energies related to the oxidation of $Nd_2Fe_{14}B$ and to the oxidation of pure iron (125 kJ mol^{-1} after [18] and 138 kJ mol^{-1} after [19]) are of the same order of magnitude.

Other studies performed on powders using different methods (thermogravimetry [20], oxygen pressure measurements [21] and thermomagnetic measurements [22]) reported very different 'apparent activation energies' (respectively 14.6 kJ mol^{-1} below 250 °C and 27.2 kJ mol^{-1} above 250 °C [20], 25 kJ mol^{-1} in the 100–250 °C range [21] and 35–50 kJ mol^{-1} in the 360–600 °C range [22]). In each case, the experimental curves were fitted with no explicit theoretical model (that is, with no relationship between the measured physical quantity and the time through a temperature-dependent coefficient). Thus, insofar as these measurements were not linked to the diffusivity and because the relationship between the temperature-dependent coefficient and the activation energy is not clearly indicated, the corresponding 'apparent activation energies' cannot be compared to our results.

6. Summary and conclusion

The oxidation kinetics of powdered Nd–Fe–B magnets in ambient air atmosphere were determined in the range 150–300 °C by Mössbauer spectrometry. In this temperature range, the intergranular diffusion of oxygen is much faster than the intragranular diffusion in bulk magnets. However, it has been shown that, for powders sieved to less than 20 μm, the particles are single $Nd_2Fe_{14}B$ grains and what is observed is the dissociation of the $Nd_2Fe_{14}B$ phase, due purely to diffusion of oxygen through the oxide. A good fit of the experimental curves was obtained according to the Ginstling–Brounshtein model, by taking into account the particle size distribution. The kinetic parameters (both the activation energy and the diffusivity pre-exponential factor) were determined to be 110 kJ mol^{-1} and 2.4 mm^2 s^{-1} respectively. These values are consistent with the values obtained at high temperature (for which the intragranular diffusion dominates) by direct measurements of the thickness of the oxidized layer by SEM.

It was shown that the kinetics parameters can be determined according to a simple single-particle analysis model (Jander's model), which seems to compensate for the effects of the particle size distribution. By using this model, it was found that the dissociation of the $Nd_2Fe_{14}B$ phase at 300 °C can be followed for powders sieved to 20–40 μm as well. However, for bigger particles (corresponding to powders sieved to 40–63 and 63–100 μm), the influence of the intergranular diffusion cannot be neglected and it is not possible to measure the kinetics parameters. From these results, Mössbauer spectrometry appears to be an accurate method for the determination of the oxidation kinetics of the $Nd_2Fe_{14}B$ phase in the 150–300 °C temperature range, complementary to SEM measurements in the 360–600 °C temperature range.

Acknowledgments

The authors would like to thank Dr D S Edgley and Professor I R Harris (University of Birmingham) for providing the samples. They are also grateful to Professor A M Huntz (Université d'Orsay) and Professor D Blavette (Université de Rouen) for helpful discussions.

References

[1] Cygan D F and McNallan M J 1995 *J. Magn. Magn. Mater.* **139** 131
[2] Le Breton J M and Teillet J 1990 *IEEE Trans. Magn.* **26** 2652
[3] Legras L 1994 *PhD Thesis* Université de Rouen
[4] Edgley D S, Le Breton J M, Lemarchand D, Harris I R and Teillet J 1993 *J. Magn. Magn. Mater.* **128** L1
[5] Le Breton J M, Teillet J, McGuiness P, Edgley D S and Harris I R 1992 *IEEE Trans. Magn.* **28** 2157
[6] Le Breton J M and Teillet J 1994 *Hyperfine Interactions* **94** 1909
[7] Tenaud P, Vial F, Barzasi A, Duchene A and Sagawa M 1990 *Proc. 11th Int. Workshop on Rare Earth Magnets and their Applications, Pittsburgh* ed S G Sankar, p 123
[8] Blanck R and Adler E 1987 *Proc. 9th Int. Workshop on Rare Earth Magnets and their Applications, Bad Soden* ed C Herget and R Poerschke, p 537
[9] Teillet J and Varret F 1983 Unpublished MOSFIT program
[10] Le Breton J M, Edgley D S, Steyaert S and Teillet J 1996 to be published
[11] Ginstling A M and Brounshtein B I 1950 *J. Appl. Chem. USSR* (English translation) **23** 1327
[12] Edgley D S, Le Breton J M, Steyaert S, Ahmed F M, Harris I R and Teillet J 1996 to be published
[13] Geiss E A 1963 *J. Am. Ceram. Soc.* **46** 374
[14] Mintz M H and Zeiri Y 1994 *J. Alloys Compounds* **216** 159
[15] Valensi G 1936 *C. R. Acad. Sci. Paris* **202** 309
[16] Jander W 1927 *Z. Anorg. Allgemeine Chem.* **163** 1
[17] Hulbert S F 1969 *Br. Ceram. Soc.* **6** 11
[18] Stewart M, Roebuck B and Gee M G 1991 *J. Mater. Sci.* **26** 1401
[19] Kubachewski O and Hopkins B E 1962 *Oxidation of Metals and Alloys* (London: Butterworths) p 108
[20] Osawa Z, Higuchi M and Hinohara S 1992 *J. Mater. Sci.* **27** 5445
[21] Higgins B E and Oesterreicher H 1987 *IEEE Trans. Magn.* **23** 92
[22] Lemarchand D, Delamare J and Vigier P 1992 *J. Appl. Phys.* **72** 1996